

First results of scientific performance for the design of ESA space based gravitational wave detector (*ELISA*)

The *Parameter Estimation Task Force*: Pau

Amaro-Seoane¹, Sofiane Aoudia¹, Gérard Auger², Stanislav Babak¹, Emanuele Berti³ Neil J. Cornish⁴, Jonathan Gair⁵, Ryan Lang⁶, Tyson Littenberg⁶, Sean McWilliams⁶, Oliver Jennrich⁷, Philippe Jetzer⁸, Ioannis Kamaretsos⁹, Antoine Klein⁸, Gijs Nelemans¹⁰, Frank Ohme¹, Eric Pagnol², Antoine Petiteau¹, Edward K. Porter², Emma Robinson¹, B. S. Sathyaprakash⁹, Bernard Schutz¹, Alberto Sesana¹, Carlos Sopuerta¹¹, Alessandro Spallicci¹², Ira Thorpe⁶, Michele Vallisneri^{13,14}, Alberto Vecchio¹⁵, Marta Volonteri¹⁶

¹ Max-Planck-Institut für Gravitationsphysik (Albert-Einstein-Institut), Am Mühlenberg 1, D-14476 Golm bei Potsdam, Germany

² APC, UMR 7164, Univ. Paris 7 Denis Diderot, 10, rue Alice Domon et Leonie Duquet, 75025 Paris Cedex 13, France

³ University of Mississippi, USA

⁴ Dept. of Physics, Montana State Univ., Bozeman, MT 59717, USA

⁵ Inst. of Astronomy, Univ. of Cambridge, Madingley Rd., Cambridge, CB30HA, UK

⁶ Gravitational Astrophysics Lab., NASA Goddard Space Flight Center, 8800 Greenbelt Rd., Greenbelt, MD 20771, USA

⁷ European Space Agency

⁸ Institute of Theoretical Physics, University of Zurich

⁹ School of Physics and Astronomy, Cardiff Univ., 5, The Parade, Cardiff, CF243YB, UK

¹⁰ Department of Astrophysics, Radboud University Nijmegen, The Netherlands

¹¹ Institute of Space Sciences (ICE-CSIC), Barcelona, Spain

¹² University of Orleans, France

¹³ Jet Propulsion Laboratory, California Inst. of Technology, Pasadena, CA 91109, USA

¹⁴ Theoretical Astrophysics, California Inst. of Technology, Pasadena, CA 91125

¹⁵ School of Physics and Astronomy, Univ. of Birmingham, Edgbaston, Birmingham B152TT, UK

¹⁶ University of Michigan

E-mail: Antoine.Petiteau@aei.mpg.de, porter@apc.univ-paris7.fr

Abstract.

This document collects the current results of

<i>CONTENTS</i>	2
-----------------	---

Contents

1 Instrument configurations : noises, orbits and sensitivity	2
1.1 Overview	2
1.2 Noises	2
1.2.1 Acceleration noises	3
1.2.2 Shot noise	4
1.2.3 Other measurement noises	4
1.2.4 Laser noise	4
1.3 Orbits	4
1.3.1 LISA like orbits	5
1.3.2 Halo around L1	5
1.4 Noise power spectral density (PSD)	7
1.4.1 Analytical model	7
1.4.2 Simulation	7
1.5 Sensitivity	7
1.5.1 Analytical model	7
1.5.2 Simulation	7
2 Galactic binaries : confusion noise and galactic binaries	10
3 Massive Black Hole binaries	10
3.1 Parameter estimation	10
3.1.1 PhenomC results from AEI (S. Babak, A. Petiteau, A. Sesana, F. Ohme, E. Robinson)	10
3.2 Model selection	10
4 EMRIs	10

1. Instrument configurations : noises, orbits and sensitivity

(‘section captain’ : *Antoine Petiteau*)

1.1. Overview

During the “first phase” (before CDF), 6 configurations had been defined. The table 1 gives a summary of their main characteristics and the induced noise levels.

1.2. Noises

The noise models used for the new space-based gravitational wave detector supported by ESA have been provided by ESA. Each noise includes the standard ESA margin $M_{ESA} = 1/0.65$.

In the following description, we give the general formulation of the root mean square value (RMS), i.e. square root of the power spectral density (PSD) in the standard unit of the noise. We also give the value used for each configurations in relative frequency unit $\frac{\delta\nu}{\nu}$.

The conversion between rms noise, δx , and power spectral density S is : $S = \delta x^2$.

Configuration	C5	C4	C3	C2	C1	HL1
Armlength ($\times 10^9$ m)	2	3	1	1	1	1 - 1.6
Orbits	analytic	analytic	analytic	10°	closest	20°
Diameter telescope (m)	0.28	0.25	0.25	0.4	0.4	0.25
Laser power (W)	2	0.7	0.7	2	0.05	0.7
Acceleration system	DRS	DRS	DRS	DRS	LPF ⁽¹⁾	DRS
Acceleration ($10^{-48} f^{-2} \text{Hz}^{-1}$)	6	6	6	6	$8.2 \left(1 + \frac{1.8 \times 10^4}{f^2}\right)^2$	6
Shot noise ($10^{-38} f^2 \text{Hz}^{-1}$)	2.05	20.07	2.31	0.06 ⁽²⁾	4.92	2.31
Fixed noise ($10^{-38} f^2 \text{Hz}^{-1}$)	2.81	2.81	2.81	2.81	2.81	2.81

Table 1. Summary of configuration. Noises are given in $\delta\nu/\nu$ unit.

Notes about particular cases including mistakes : (1) the margin has been taken into account 2 times ; (2) the laser power has been considered in the rms shot noise with power -1 instead of -0.5 .

The conversion between acceleration noise unit (in $\text{m}^2 \cdot \text{s}^{-4} \cdot \text{Hz}^{-1}$) and noise in length unit (in $\text{m}^2 \cdot \text{Hz}^{-1}$) is :

$$S(f) = S_{\text{m}^2 \cdot \text{s}^{-4} \cdot \text{Hz}^{-1}}(f) / (2\pi f)^4 \text{ m}^2 \cdot \text{Hz}^{-1} \quad (1)$$

The conversion between noise in length unit ($\text{m}^2 \cdot \text{Hz}^{-1}$) and noise in relative frequency unit (in Hz^{-1}) is :

$$S_{\frac{\delta\nu}{\nu}}(f) = S(f) \times \left(\frac{2\pi f}{c}\right)^2 \text{ Hz}^{-1} \quad (2)$$

1.2.1. Acceleration noises This noise is due to the limitation of the drag-free system. We consider two types of acceleration noise :

- DRS : acceleration noise corresponding to LISA requirements :

$$\delta x_{\text{acc}}^{\text{DRS}} = M_{ESA} \times 3 \times 10^{-15} \text{m/s}^2 / \sqrt{\text{Hz}} \quad (3)$$

- LPF : acceleration noise corresponding to LISAPathfinder :

$$\delta x_{\text{acc}}^{\text{LPF}} = M_{ESA} \times 3.5 \times 10^{-15} \left(1 + \frac{0.18 \text{ mHz}}{f}\right) \text{m/s}^2 / \sqrt{\text{Hz}} \quad (4)$$

So, we have one best case, the DRS, and one worth case, the LPF.

Note that for the LPF noise, we include the ESA margin but, according to Stefano Vitale, the margin was already taken into account in the 3.5×10^{-15} value. So the LPF acceleration was over-estimated (only used for configuration C1).

The acceleration noise for the different configurations is :

- for C1 :

$$S_{\text{acc}, \frac{\delta\nu}{\nu}}(f) = 8.17 \times 10^{-48} \left(\frac{1}{f} + \left(\frac{1.8 \times 10^{-4}}{f^2}\right)\right)^2 \text{Hz}^{-1} \quad (5)$$

- for C2, C3, C4, C5, HL1 :

$$S_{\text{acc}, \frac{\delta\nu}{\nu}}(f) = 6.00 \times 10^{-48} f^{-2} \text{Hz}^{-1} \quad (6)$$

1.2.2. Shot noise This noise depends directly on the received laser power after the travel between two spacecrafts. Therefore it depends on :

- L : the armlength (in m),
- D : the diameter of the telescope (in m),
- P : the emitted laser power (in Watt)

$$\delta x_{\text{SN}} = M_{ESA} \times 7.7 \times 10^{-12} \left(\frac{1 \text{ W}}{P} \right)^{1/2} \left(\frac{L}{5 \times 10^9 \text{ m}} \right) \left(\frac{0.4 \text{ m}}{D} \right)^2 \text{ m}/\sqrt{\text{Hz}} \quad (7)$$

The acceleration noise for the different configurations is :

- for C1 :

$$S_{SN, \frac{\delta\nu}{\nu}}(f) = 4.92 \times 10^{-38} f^2 \text{ Hz}^{-1} \quad (8)$$

- for C2 :

$$S_{SN, \frac{\delta\nu}{\nu}}(f) = 6.14 \times 10^{-40} f^2 \text{ Hz}^{-1} \quad (9)$$

- for C3 :

$$S_{SN, \frac{\delta\nu}{\nu}}(f) = 2.31 \times 10^{-38} f^2 \text{ Hz}^{-1} \quad (10)$$

- for C4 :

$$S_{SN, \frac{\delta\nu}{\nu}}(f) = 2.07 \times 10^{-37} f^2 \text{ Hz}^{-1} \quad (11)$$

- for C5 :

$$S_{SN, \frac{\delta\nu}{\nu}}(f) = 2.05 \times 10^{-38} f^2 \text{ Hz}^{-1} \quad (12)$$

- for HL1 :

$$S_{SN, \frac{\delta\nu}{\nu}}(f) = 2.31 \times 10^{-38} f^2 \text{ Hz}^{-1} \quad (13)$$

1.2.3. Other measurement noises This noise groups to the perturbation of the optical path in the optical bench and the telescope and the precision on the interference measurement by the photodiode and the phasemeter.

$$\delta x_{\text{OMS}} = M_{ESA} \times 6.2 \times 10^{-12} \text{ m}/\sqrt{\text{Hz}} \quad (14)$$

The other measurement noise is the same for all the configurations :

- for C1,C2, C3, C4, C5, HL1 :

$$S_{OMS, \frac{\delta\nu}{\nu}}(f) = 2.81 \times 10^{-38} f^2 \text{ Hz}^{-1} \quad (15)$$

1.2.4. Laser noise The laser noise which have a typical rms noise around $30 \text{ Hz} \cdot \text{Hz}^{-1/2}$ is reduced by the Time Delay Interferometry method. For this study, we suppose that the application of TDI second generation reduce the laser noise below the other noise. So it will not be consider.

1.3. Orbits

We use several spacecraft orbits divided in 2 types : LISA like orbits and Halo around Lagrange point L1. There are 2 key points :

- the stability of the constellation which have implication to the mission duration and on the shot noise level (see 1.2.2).
- the way of reaching the orbits which have direct budget link through the energy required

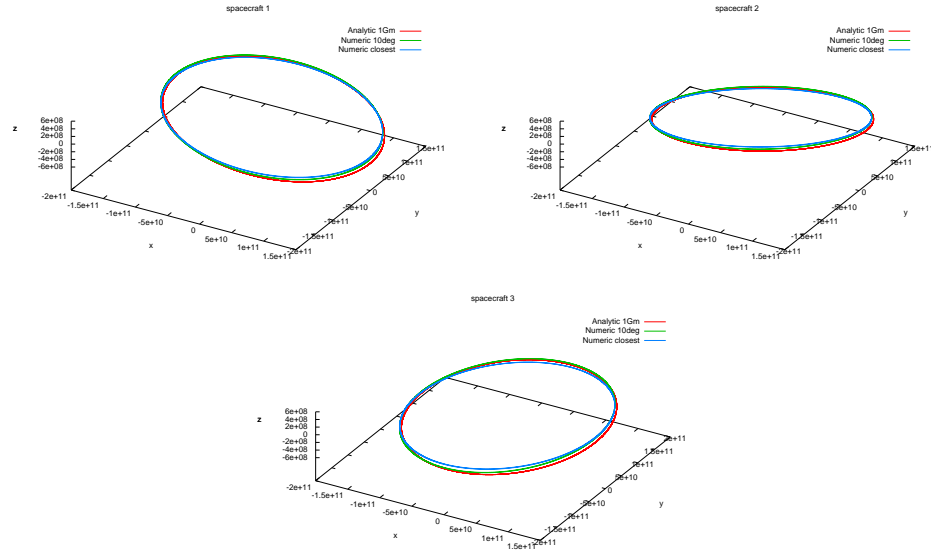


Figure 1. Orbits of the 3 spacecrafts.

1.3.1. LISA like orbits The LISA like orbits corresponds to constellation in a pseudo-equilateral triangle. The barycenter of the constellation follows the Earth with a certain Earth-detector barycenter angle, θ_{EdB} . For this type of orbits, the constellation 2 key points are the armlength and the angle θ_{EdB} . To keep the stability, if we want to increase the armlength, it implies an increase of θ_{EdB} for limiting the tidal deformation due to the Earth.

We test 2 orbits which are the output of numerical simulation done by Oliver Jennrich (ESA) :

- best case : $\theta_{EdB} = 10^\circ$ and $L = 10^9$ m,
- worst case : closest to the Earth ($\theta_{EdB} = ??^\circ$) and $L = 10^9$ m,

We also use the standard analytical LISA orbits from [2] changing the armlength.

The figure 1 shows the numerical orbits compared to the analytic orbits with $L = 10^9$ m. Regarding the position of the spacecraft the numerical orbits are close to the analytic ones. This means that the analytic orbits are a good approximation to the numeric one for computing the response of the detector to gravitational waves.

The main difference between this orbits is the time variation of the armlength as shown on the figure ???. This is an important point for the technological design of the detector (Doppler effect, ...) and for the application of the Time Delay Interferometry which is the pre-data-analysis method for reducing the laser noise.

1.3.2. Halo around L1 We test another kind of orbits : the Halo around Lagrange point L1. This orbits are the results of numerical simulation done by Vitali Mueller (AEI-Hannover). It's a mother/daughter configuration : there are only 4 links (2 arms). The figure 3 shows the orbits and the figure 4 shows the armlength evolution.

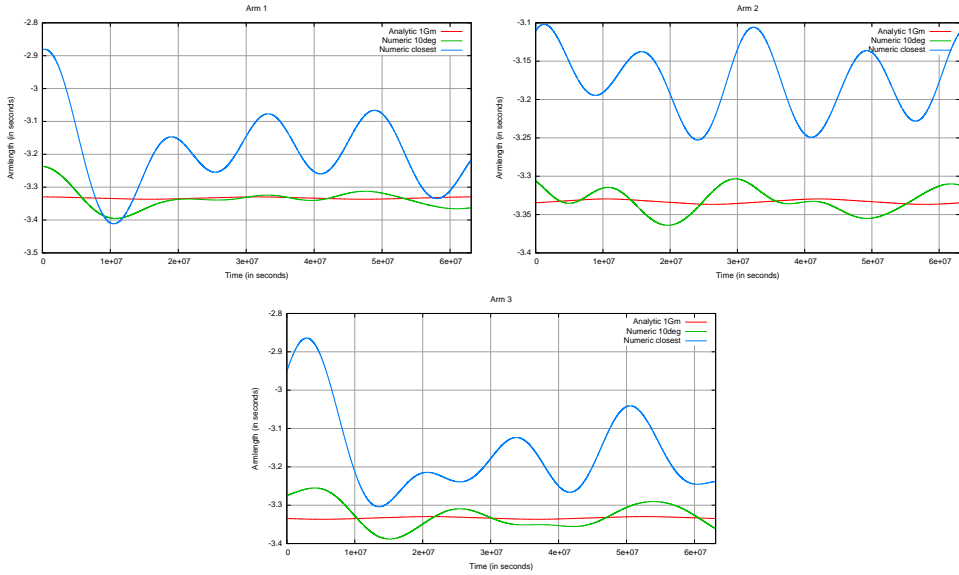


Figure 2. Time evolution of the 3 arm length during 2 years.

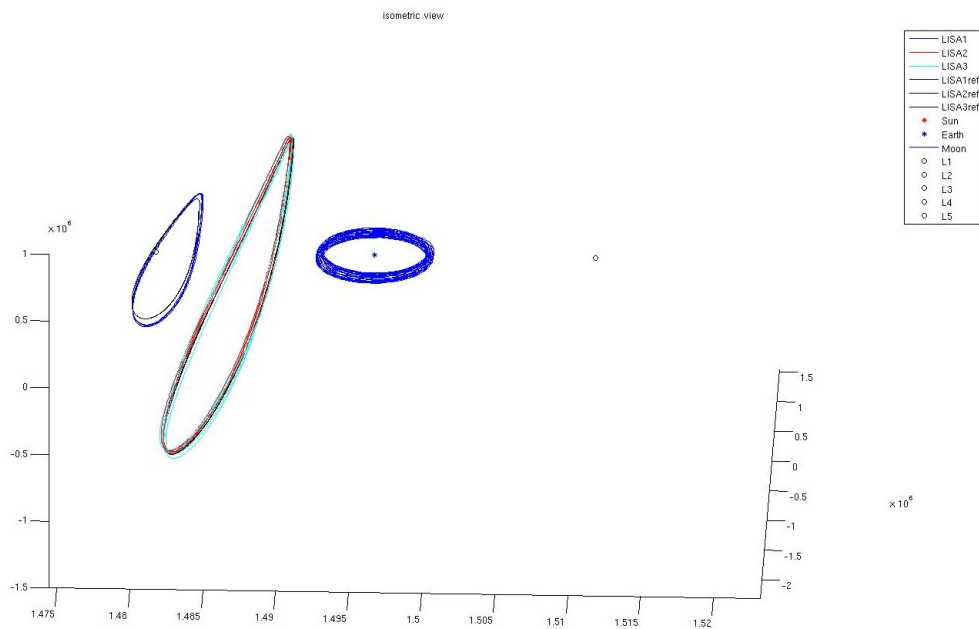


Figure 3. Orbit of spacecraft for the Halo around L1 configuration.

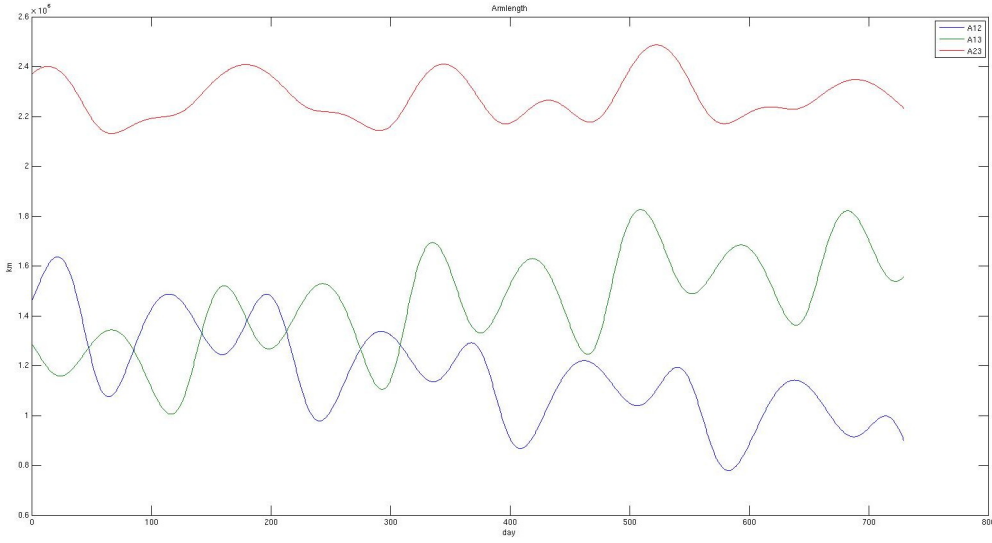


Figure 4. Evolution of armlength for the Halo around L1 configuration.

The main spacecraft (mother) is on a close orbit around L1 and the 2 daughters are on a distant orbits separated in phase by π . The angle between the 2 arms is around 120° . The armlengths evolve between 1 and 1.6 million km.

1.4. Noise power spectral density (PSD)

1.4.1. Analytical model The analytic formulation of the Power Spectral Density of TDI X can be approximated by (usual approximation used in LISA) :

$$S_{n,\frac{\delta\nu}{\nu}}^X(f) = 16 * \sin^2(\phi_L(f)) \left(S_{SN,\frac{\delta\nu}{\nu}}(f) + S_{OMN,\frac{\delta\nu}{\nu}}(f) + (3 + \cos(2\phi_L(f))) S_{acc,\frac{\delta\nu}{\nu}}(f) \right) \quad (16)$$

with $\phi_L(f) = 2\pi f L/c$

1.4.2. Simulation

1.5. Sensitivity

1.5.1. Analytical model (Very) approximative analytic formulation (based on LISA science requirements document (2010)) :

The transfert function is

$$T(f) = \sqrt{1 + \left(\frac{f}{(0.41 \left(\frac{c}{2L} \right))} \right)^2} \quad (17)$$

Sensitivity formulation :

$$\sqrt{S_h^X(f)} = \sqrt{5} \frac{2}{\sqrt{3}} T(f) \frac{\sqrt{4S_{acc} + S_{SN} + S_{omn}}}{L} \quad (18)$$

1.5.2. Simulation

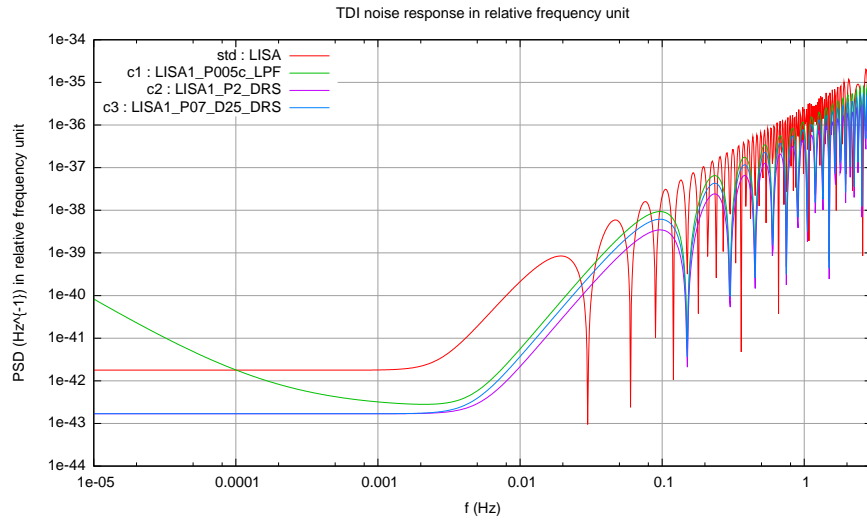


Figure 5. Comparison of power spectral density of noises' response for standard LISA, configurations 3a, 4a and 5a

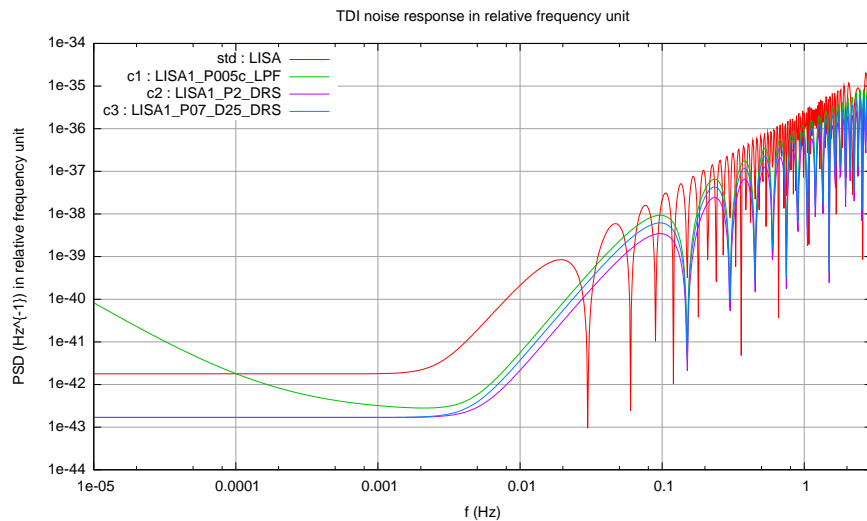


Figure 6. Comparison of power spectral density of noises' response for standard LISA, configurations 1c, 2 and 3

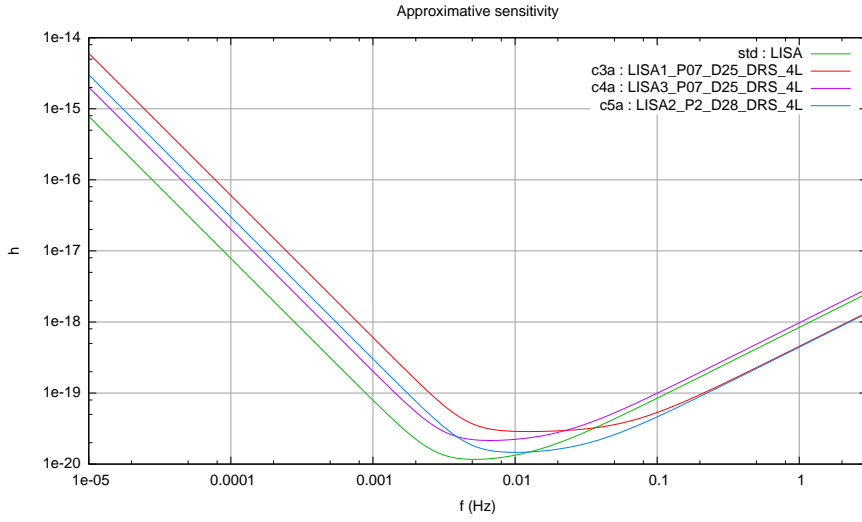


Figure 7. Comparison of sensitivity (SNR=1, "instantaneous") for standard LISA, configurations 3a, 4a and 5a

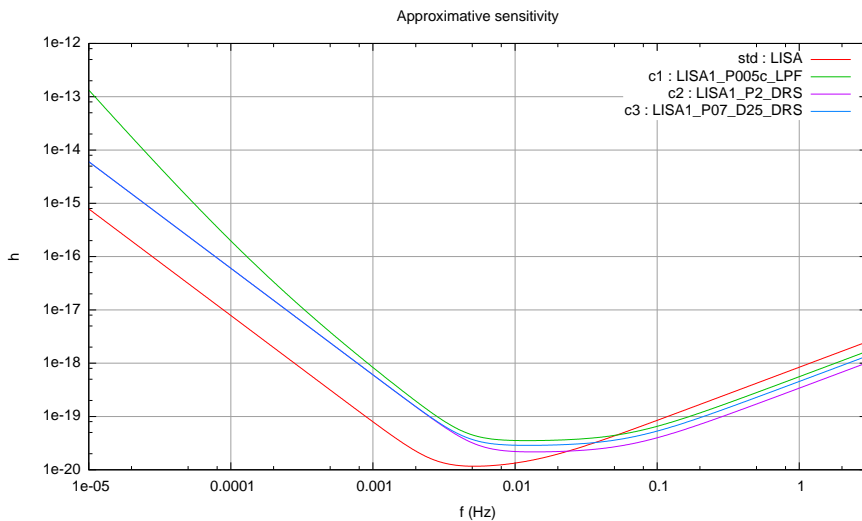


Figure 8. Comparison of sensitivity (SNR=1, "instantaneous") for standard LISA, configurations 1c, 2 and 3

2. Galactic binaries : confusion noise and galactic binaries

(*'section captain'* : *Tyson Littenberg*)

3. Massive Black Hole binaries

(*'section captain'* : *Alberto Sesana*)

3.1. Parameter estimation

(*'section captains'* : *Neil Cornish & Emanuele Berti*)

3.1.1. PhenomC results from AEI (*S. Babak, A. Petiteau, A. Sesana, F. Ohme, E. Robinson*) We use PhenomC waveforms described in [1]. Waveforms include merger and ringdown and assume aligned spins. Given the latter assumption, we apply them to efficient accretion models (SE, LE) only. Moreover, since the waveforms can not handle too extreme cases, we lower the maximal spin limit to 0.98, and considered only sources with mass ratio larger than $q = M_2/M_1 = 0.05$, thus loosing 10-20% of the sources (depending on the MBH population model) in our analysis.

We consider a threshold SNR= 6 for detection, and SNR= 10 for trustworthy parameter estimations. We show results for detectors LISA, C4, C5, C2, C3 and C5, assuming a single Michelson interferometer.

Figures 9 and 10 show histograms of parameter estimation accuracy for the ten realizations of model SE and LE respectively with LISA, C2, C4 and C5; only sources with SNR> 10 are included.

The median parameter estimation accuracy with LISA, C2, C4 and C5 as a function of redshift is shown in figures 13-to-14.

The median source SNR with LISA, C2, C4 and C5 as a function of redshift is shown in figures 13-to-14.

For comparison we also add results comparing about C1, C2 and LISA and SNR for C3 :

Figures 15, 16, 17 and 18 show the performances of LISA, C2 and C1 respectively, assuming the SE MBH binary population model.

Figures 19 and 20 show histograms of parameter estimation accuracy for the ten realizations of model SE and LE respectively; only sources with SNR> 10 are included.

The median source SNR and parameter estimation accuracy as a function of redshift is shown in figures 22-to-24.

3.2. Model selection

(*'section captain'* : *Alberto Sesana*)

4. EMRIs

(*'section captains'* : *Jon Gair & Ed Porter*)

- [1] L. Santamaria, F. Ohme, P. Ajith, B. Bruegmann, N. Dorband, M. Hannam, S. Husa, P. Moesta, D. Pollney, C. Reisswig, E. L. Robinson, J. Seiler and B. Krishnan, Phys. Rev. D **82**, 064016 (2010)

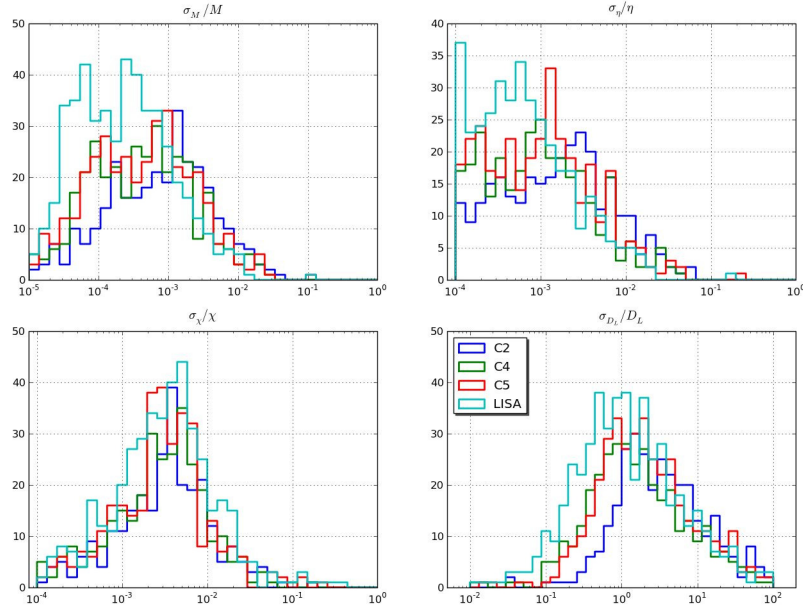


Figure 9. 1- σ errors on source parameters: redshifted mass (upper left); symmetric mass ratio (upper right); spin parameter (lower left); luminosity distance (lower right). Histograms collect all the events in the SE catalogue (small seed), with SNR> 10. Light blue histograms are for LISA, blue histograms are for C2, green histograms are for C4 and red histograms are for C5.

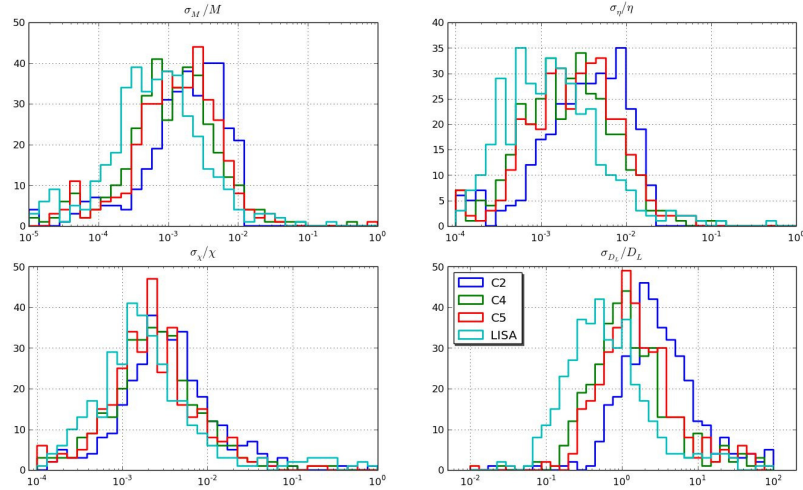


Figure 10. 1- σ errors on source parameters. Similar as 9 with LE catalogue (large seed).

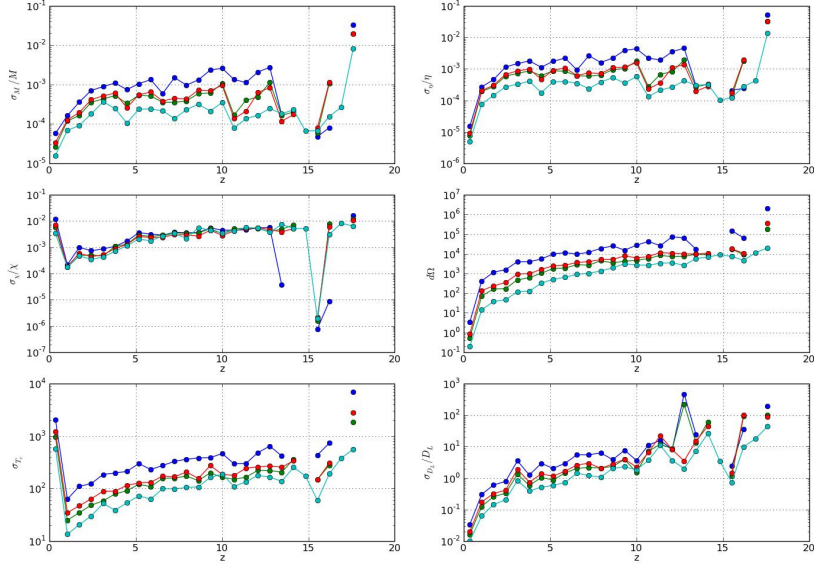


Figure 11. Median 1- σ errors on the source parameters as a function of z : redshifted mass (upper left); symmetric mass ratio (upper right); spin parameter (middle left); sky location in deg^2 (middle right); coalescence time in seconds (lower left); luminosity distance (lower right). Colorstyle as in figure 9 : light blue histograms are for LISA, blue histograms are for C2, green histograms are for C4 and red histograms are for C5. Model SE (small seeds) is assumed.

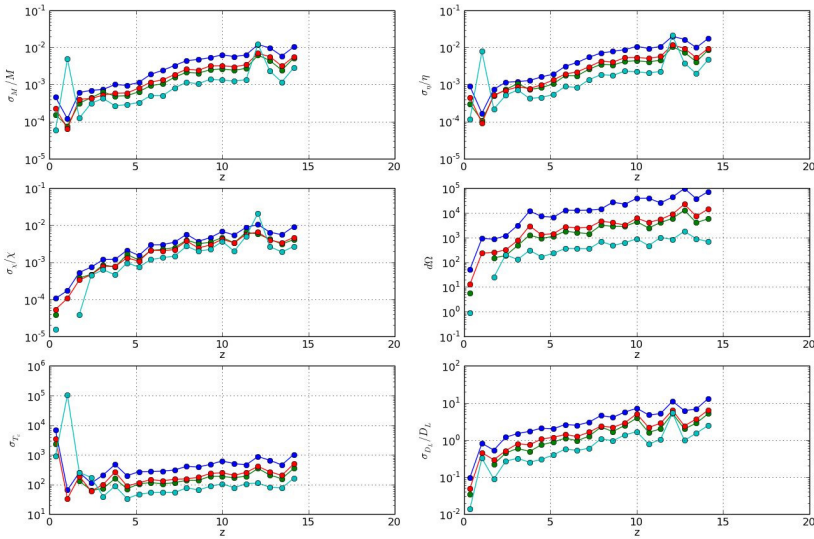


Figure 12. Same as figure 11 but for the LE (large seed) catalogue.

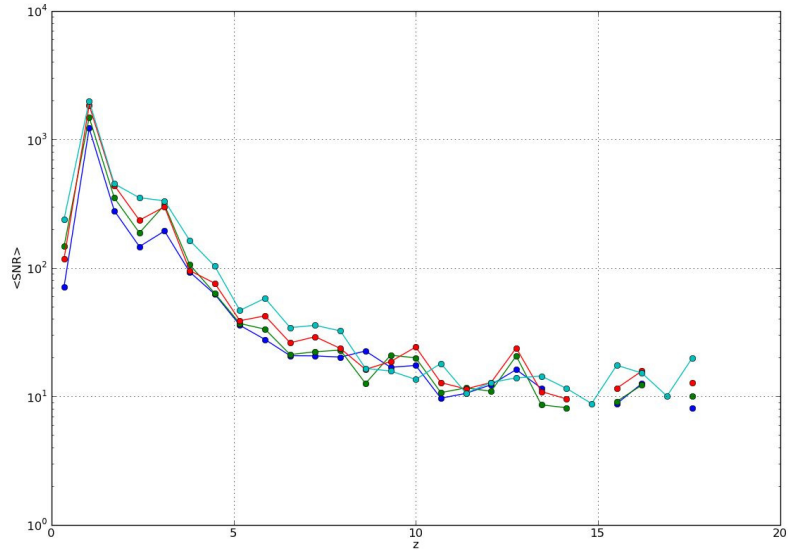


Figure 13. Median SNR s as a function of z . Colorstyle as in figure 9 : light blue histograms are for LISA, blue histograms are for C2, green histograms are for C4 and red histograms are for C5. Model SE (small seeds) is assumed.

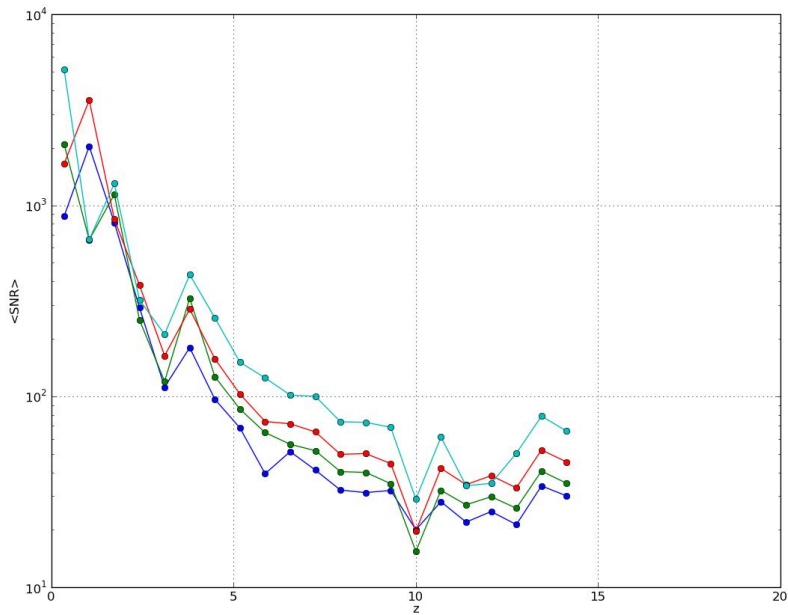


Figure 14. Same as figure 13 but for the LE (large seed) catalogue.

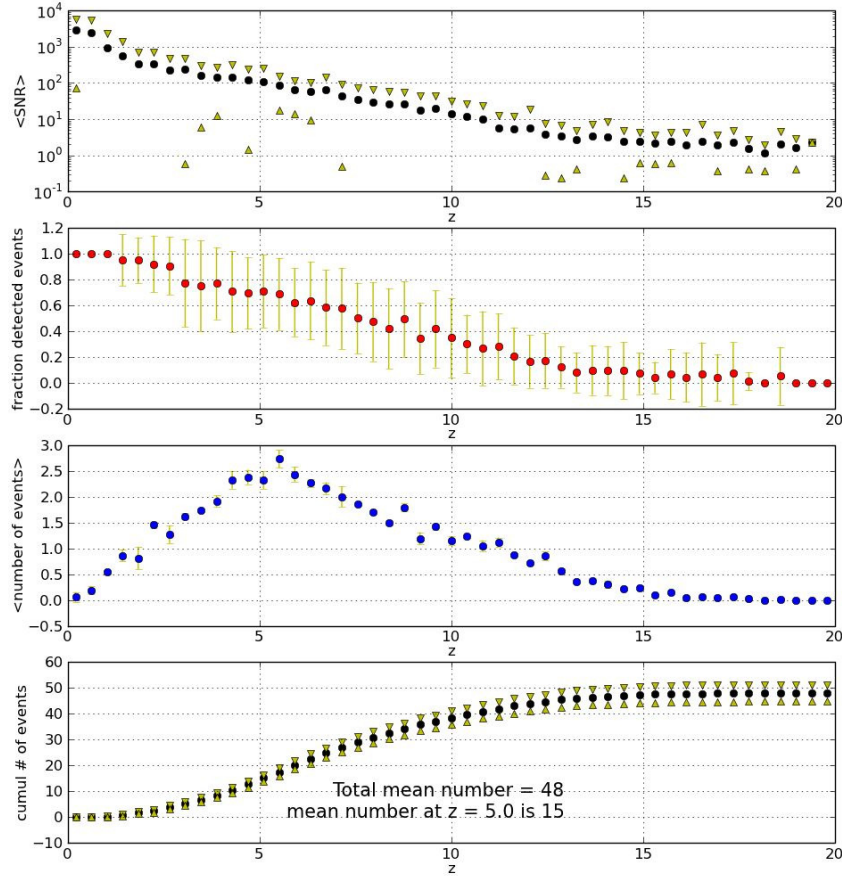


Figure 15. LISA performances as a function of redshift. From the top to the bottom we plot the average source SNR, the fraction of detectable sources ($\text{SNR} > 6$), the mean number of detected sources, and the cumulative number of detected sources. Error bars are standard deviations; SE population model is assumed.

- [2] Dhurandhar, S. V. and Nayak, K. R. and Koshti, S. and Vinet, J.-Y. Classical and Quantum Gravity **22**, 481-487 (2005)

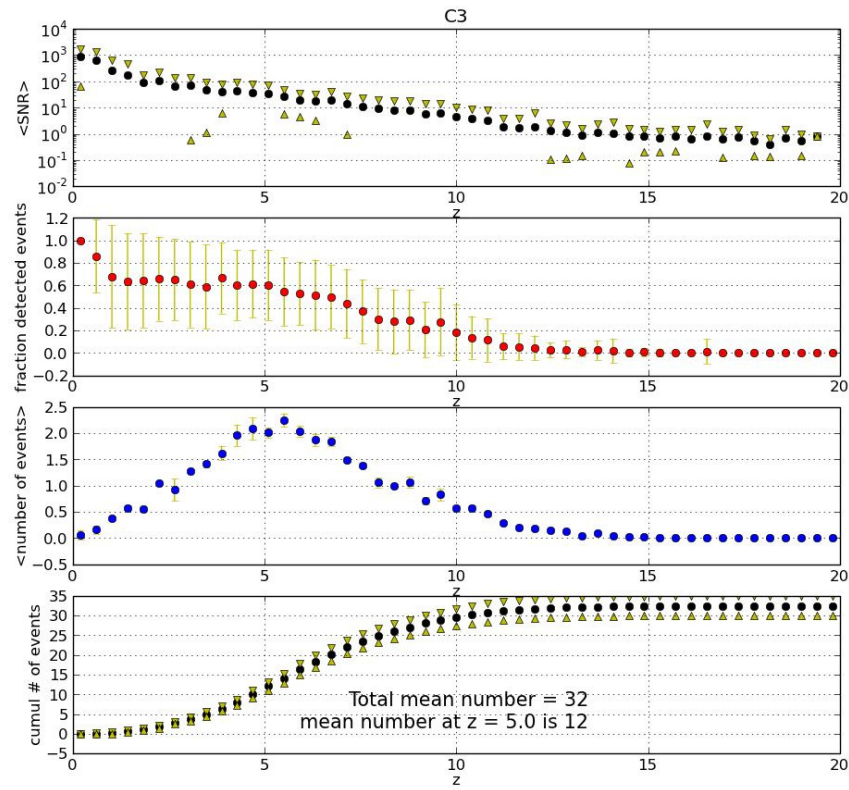


Figure 16. Same as figure 15 but for C3.

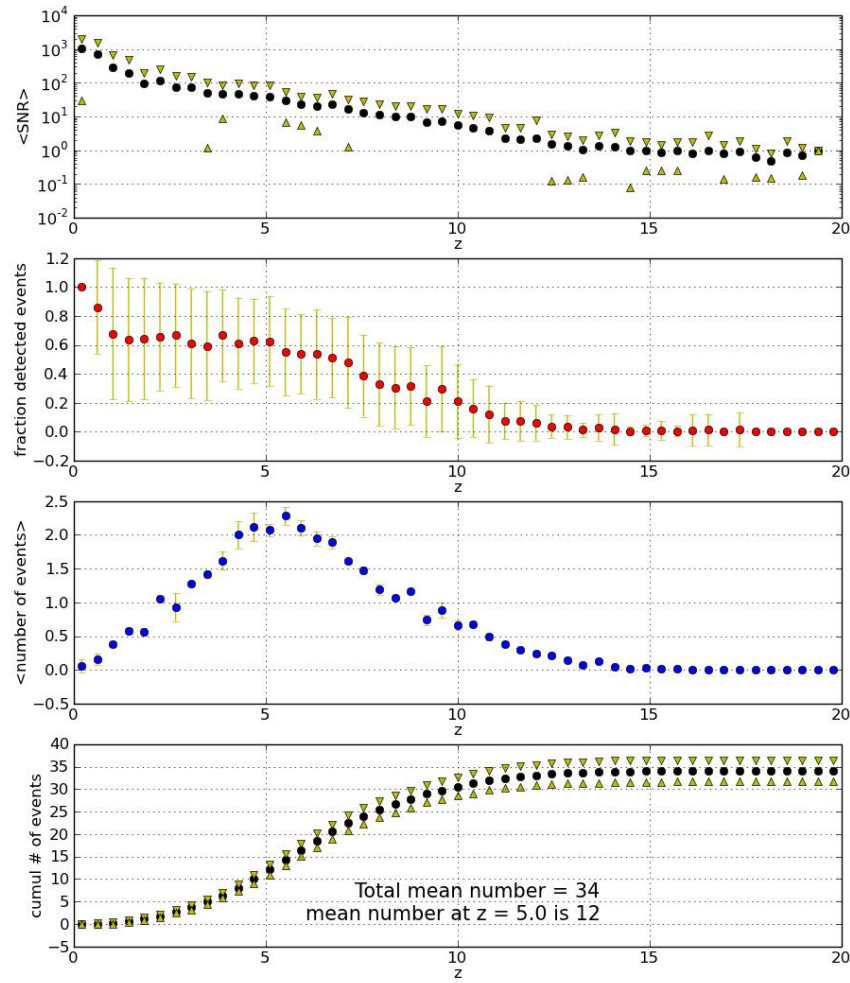


Figure 17. Same as figure 15 but for C2.

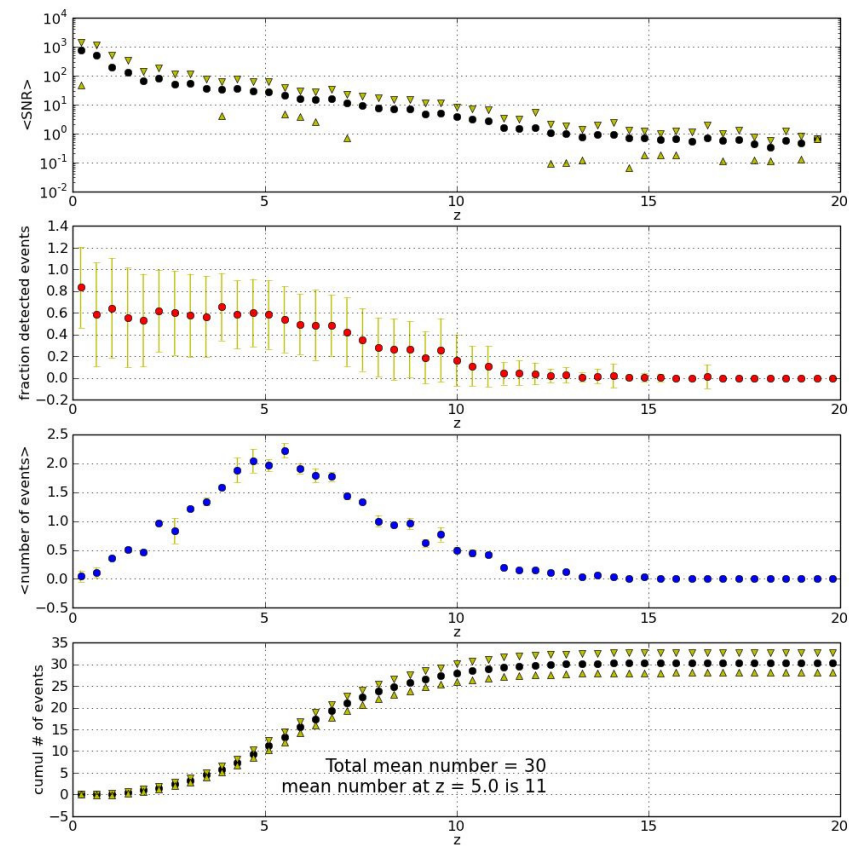


Figure 18. Same as figure 15 but for C1.

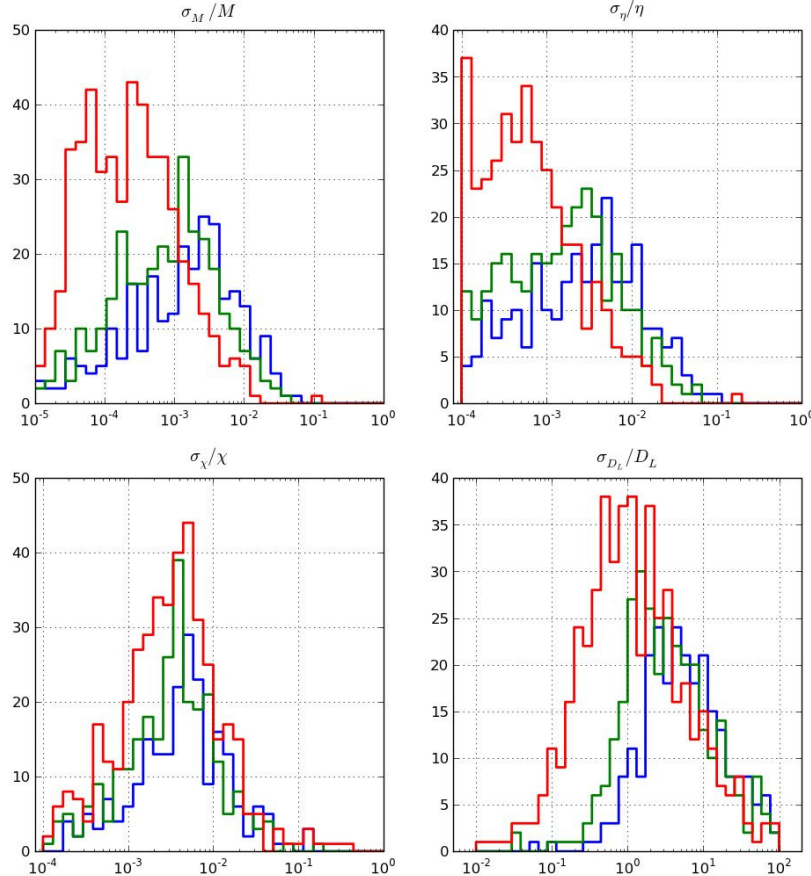


Figure 19. 1- σ errors on source parameters: redshifted mass (upper left); symmetric mass ratio (upper right); spin parameter (lower left); luminosity distance (lower right). Histograms collect all the events in the SE catalogue, with $\text{SNR} > 10$. Red histograms are for LISA, green histograms are for C2 and blue histograms are for C1.

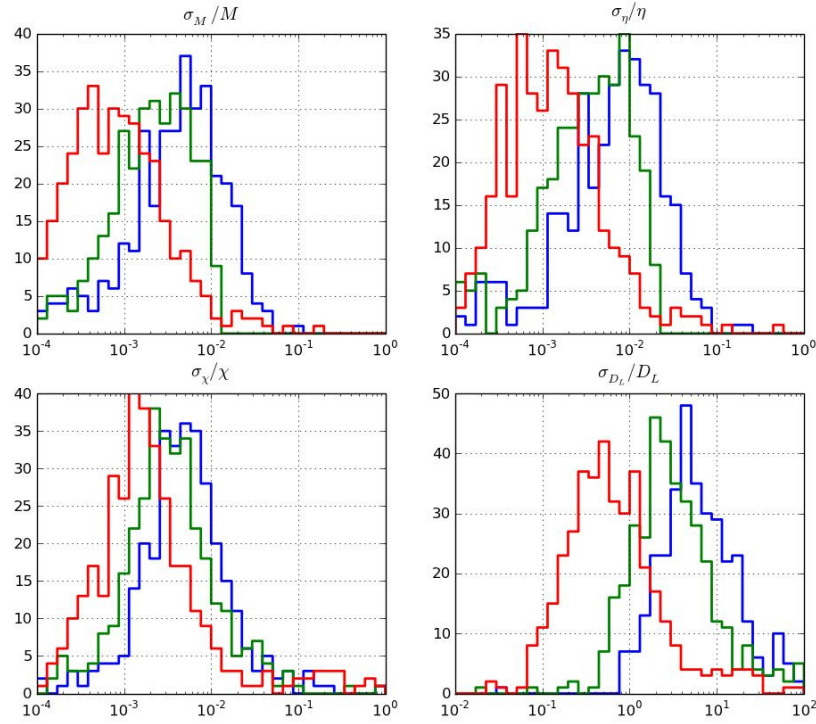


Figure 20. Same as figure 19 but for the LE catalogue.

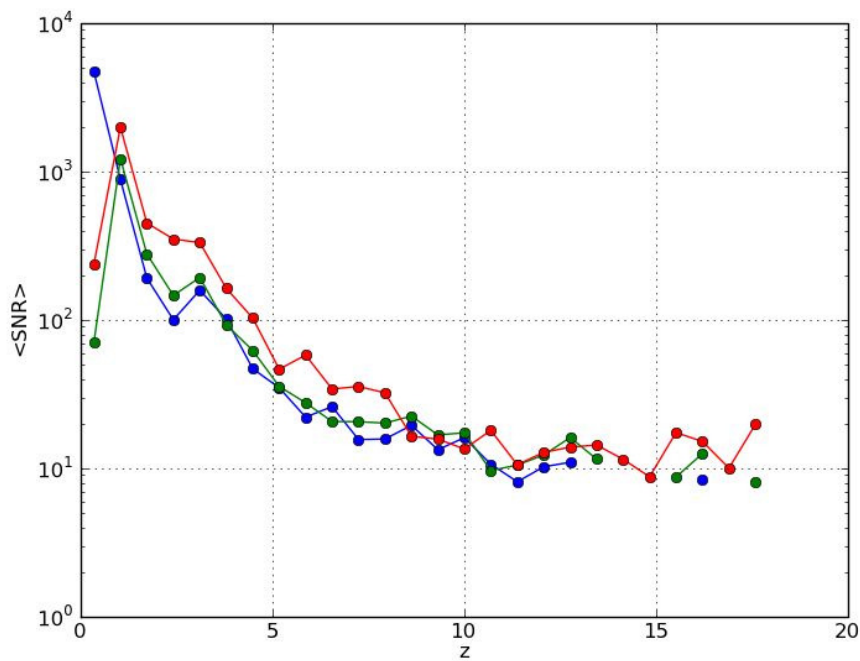


Figure 21. Median source SNR as a function of z . Colorstyle as in figure 19. Model SE is assumed.

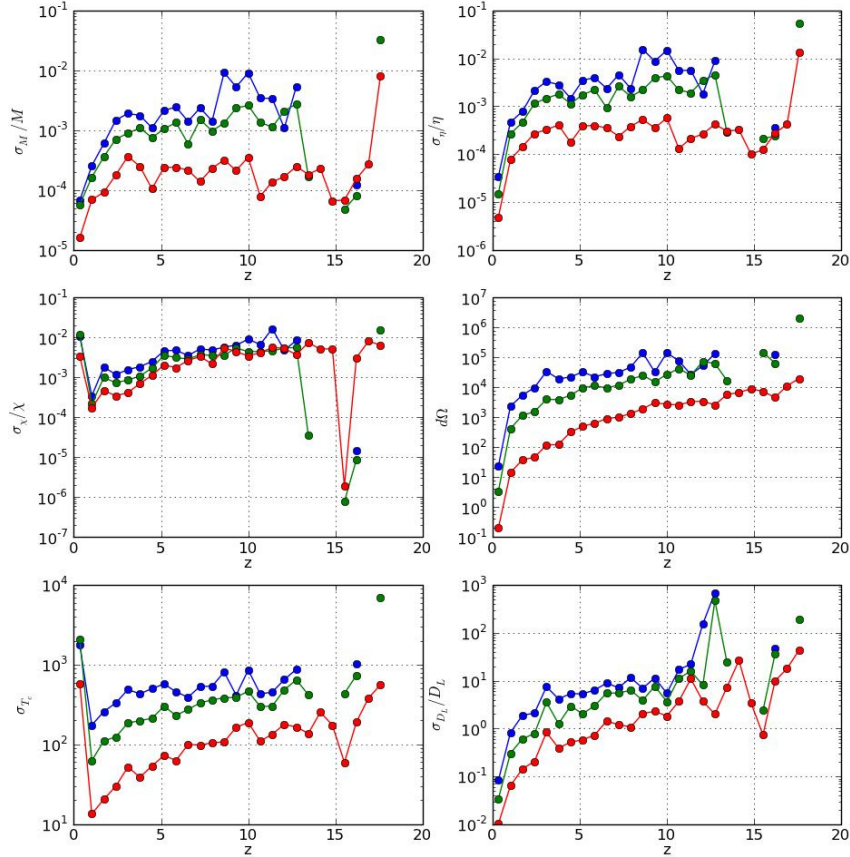


Figure 22. Median $1-\sigma$ errors on the source parameters as a function of z : redshifted mass (upper left); symmetric mass ratio (upper right); spin parameter (middle left); sky location in deg^2 (middle right); coalescence time in seconds (lower left); luminosity distance (lower right). Colorstyle as in figure ???. Model SE is assumed.

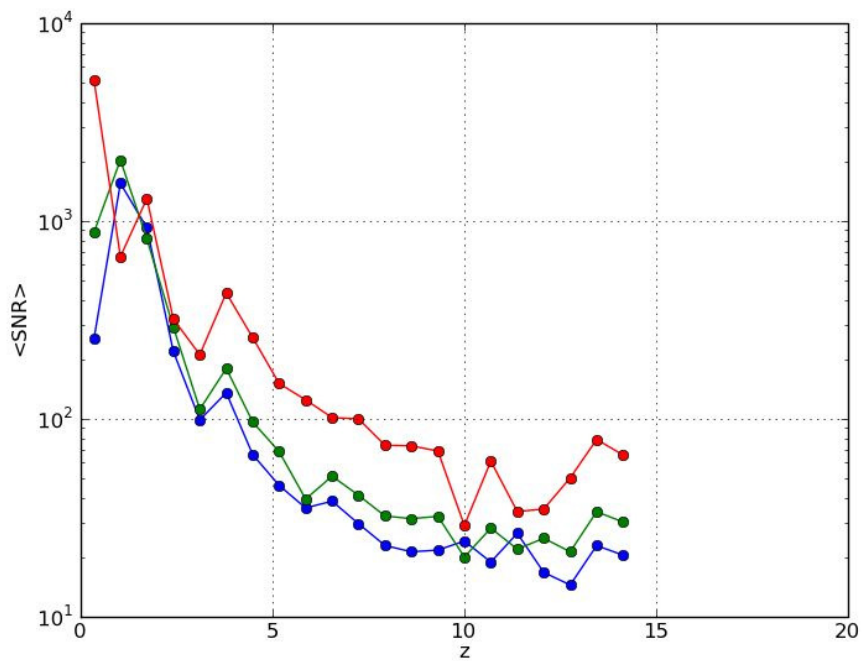


Figure 23. Same as figure 22 but for the LE catalogue.

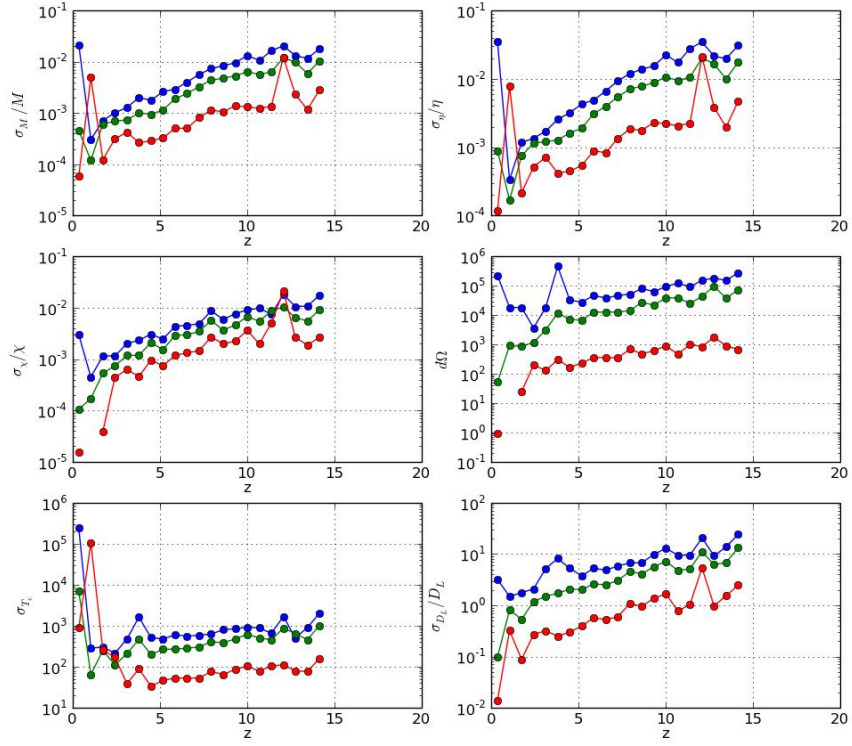


Figure 24. Same as figure 22 but for the LE catalogue.